- 3D simulations of H/He burning in X-ray bursts….feedback effects in NS nucleosynthesis

Sanjib S. Gupta (T-16,LANL)

LANL Collaborators:

Alexander Heger (T-6)

Peter Moller (T-16)

Jerome Daligault (T-15)

Sanjay Reddy (T-16)

H/He burning on the surface of Accreting NS

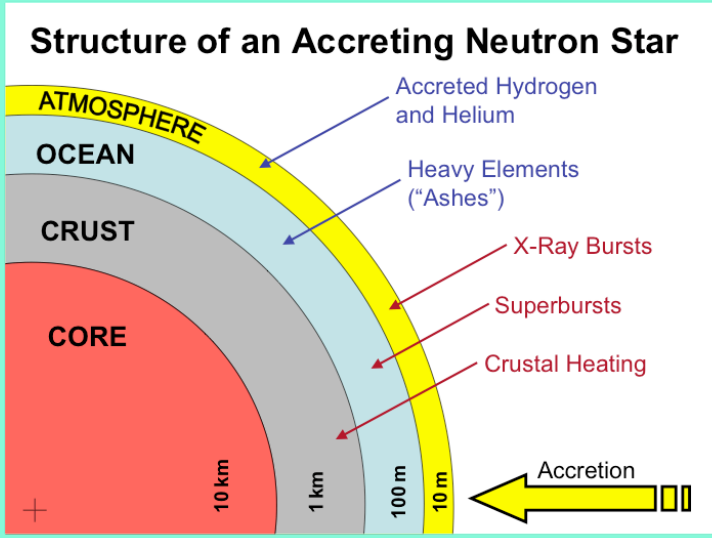

* In a LMXB system, the more massive star with shorter lifetime can leave behind a Neutron Star (NS) after core-collapse,which can accrete H/He-rich material from the low-mass companion through a disk.

*Degenerate conditions at the base of the accreted atmosphere can lead to a thermal instability if the heat lost by radiation transport (photons and free-streaming neutrinos) cannot cope with the (local) nuclear energy production.

*Hydrogen burning is ignited through the "hot-CNO" cycle, with breakout reactions such as $^{15}O(\alpha, \gamma)^{19}Ne$ at around $4 \cdot 10^8$ K . The hot-CNO-cycle is $^{12}C(p, \gamma)^{13}N(p, \gamma)^{14}O(\beta^+)^{14}N(p, \gamma)^{15}O(\beta^+)^{15}N(p, \alpha)^{12}C$, a catalytic conversion of $4\,^1H$ into ^4He

***Movement from the CNO cycles towards Fe-group nuclei** is strongly temperature dependent. At low temperature a slow "rp-process" begins with 2p-captures on an even-even nucleus, a β^+ decay, p-capture, a β^+ decay,and a final (p, α) reaction close to stability on odd-Z targets such as ^{15}N, ^{19}F, ^{23}Na, ^{27}Al, ^{31}P, ^{35}Cl: these are the nuclei at which the H-burning cycles are connected resulting in the CNO-,NeNa-,MgAl-,SiP-,SiCl-cycles. The flow to heavier elements is determined by the (p,γ)/(p, α) rate ratio into the next cycle. Burning timescales are therefore sensitive to an accurate determination of these ratios. At around $3 \cdot 10^8$ K all the sub-cycles are open except the CNO-, which awaits the $^{15}O(\alpha, \gamma)^{19}Ne$ reaction.

***Breakouts from these sub-cycles** can occur at higher temperatures via p- or α-capture on an unstable isotope in the cycle, such as the $^{15}O(\alpha, \gamma)$, $^{23}Mg(p, \gamma)$, $^{27}Si(p, \gamma)$,$^{31}S(p, \gamma)$ reactions, which limit storage times in the sub-cycles. *However, if these timescales become comparable to or exceed the macroscopic timescales then the cycle is the endpoint of the rp-process and the steady-flow abundance in the sub-cycle determines the final nucleosynthesis abundance distribution.*

*Higher temperatures from thermal feedback shift the process closer to the proton drip line (higher Coulomb barriers can be overcome) with high (p, γ) reaction rates and the *slowest reactions in the sub-cycles become the β^+ decays which act as "Waiting Points"* . The rp-process is now significantly **impeded by (γ,p) photo-disintegrations** and the proton capture process may stop altogether leading to decreasing thermal feedback and a "freezout" - i.e. if the (p, γ) rates fall below the β^+ decay rates on a nucleus it becomes substantially enriched in the freezout abundance profile - ***the "ashes of the rp-process"***

H/He burning –Part II

A further complication at high temperatures and densities, is the competition of the so-called "αp-process" when temperatures are high enough to overcome the alpha-particle Coulomb barrier. This usually populates excited states above proton thresholds so that the reaction sequence is (α,p) (p,γ). This bypassing of β-decays between even-even nuclear network nodes is seen starting at Oxygen isotopes around $4 \cdot 10^8$K upto Ar.

He burns by the 3α-reaction into ^{12}C. Apart from the thermal feedback between the H and He layers (which enhance reaction rates) there are also chemical feedback effects which can be amplified by Rayleigh-Taylor unstable "plumes" which we can model in 3D mixing. The proton captures $^{12}C(p,\gamma)^{13}N(p,\gamma)^{14}O$ are very fast, so the 3α-process enhances hot-CNO burning, whose rate depends on the mass fraction of CNO isotopes. At the same time the $^{15}N(p,\alpha)^{12}C$ reaction increases the He concentration and feeds the 3α ! Ignition in a mixed H/He burst comes from unchecked thermal feedback from the 3α-process when the EOS (which determines Pressure response and consequent entropy generation to temperature/density perturbations) is set by the degenerate electron Fermi gas (the stellar environment does not "immediately" expand and cool as in non-degenerate quiescent burning).

Depending on the thermal conditions, the hot-CNO breakout can return to ^{15}O via the hot-CNO-bicycle pathway $^{19}Ne(\beta^+)^{19}F(p,\alpha)^{16}O$ $(p,\gamma)^{17}F$ $(p,\alpha)^{18}Ne$ $(\beta^+)^{18}F(p,\alpha)^{15}O$ and accelerate conversion of Hydrogen to Helium , thus affecting the runaway.

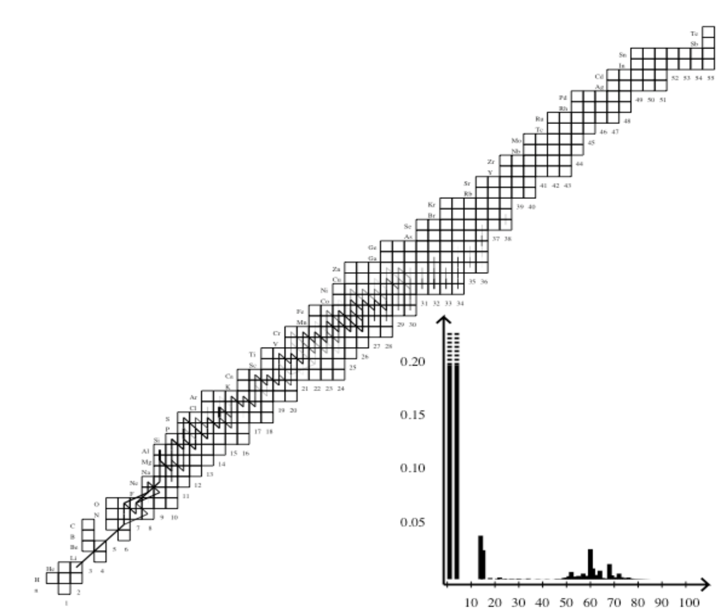

Fig. 13.— Above ignition: $T = 4.44 \cdot 10^8$K, $\rho = 3.46 \cdot 10^5$g/cm^3, $X = 0.398$, $Y = 0.402$, $t = -11.091$s. (see end of §4 for an explanation of the diagram).

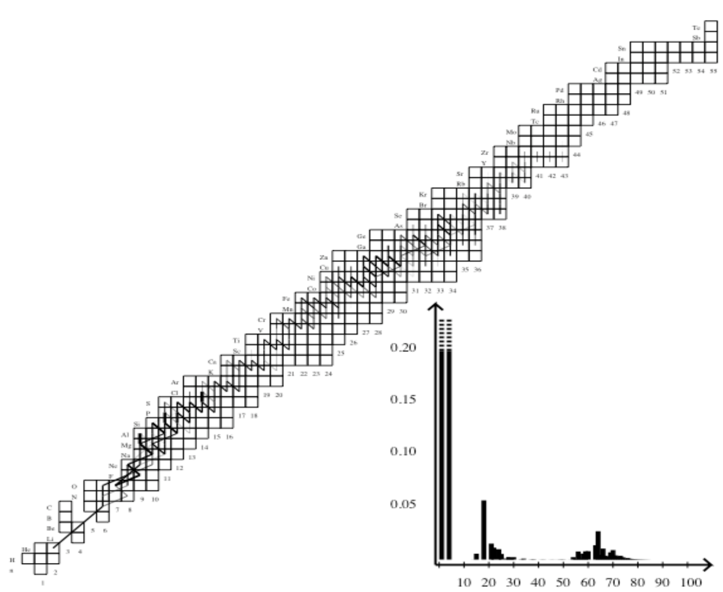

Fig. 15.— Above ignition: $T = 6.97 \cdot 10^8$K, $\rho = 2.51 \cdot 10^5$g/cm^3, $X = 0.381$, $Y = 0.372$, $t = -9.994$s. (see end of §4 for an explanation of the diagram).

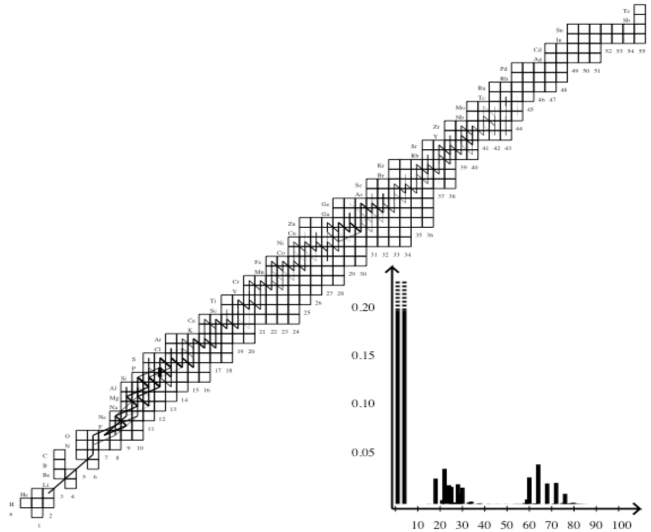

Fig. 16.— Above ignition: $T = 8.34 \cdot 10^8$K, $\rho = 2.15 \cdot 10^5$g/cm^3, $X = 0.358$, $Y = 0.346$, $t = -9.097$s. (see end of §4 for an explanation of the diagram).

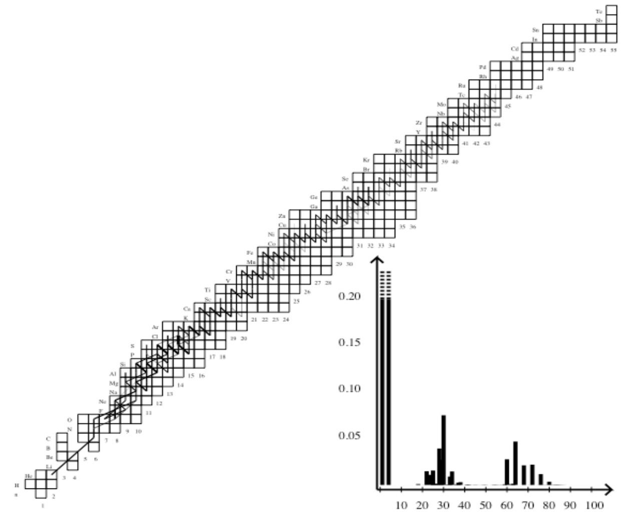

Fig. 17.— Above ignition: $T = 8.96 \cdot 10^8$K, $\rho = 2.07 \cdot 10^5$g/cm^3, $X = 0.327$, $Y = 0.326$, $t = -8.075$s. (see end of §4 for an explanation of the diagram).

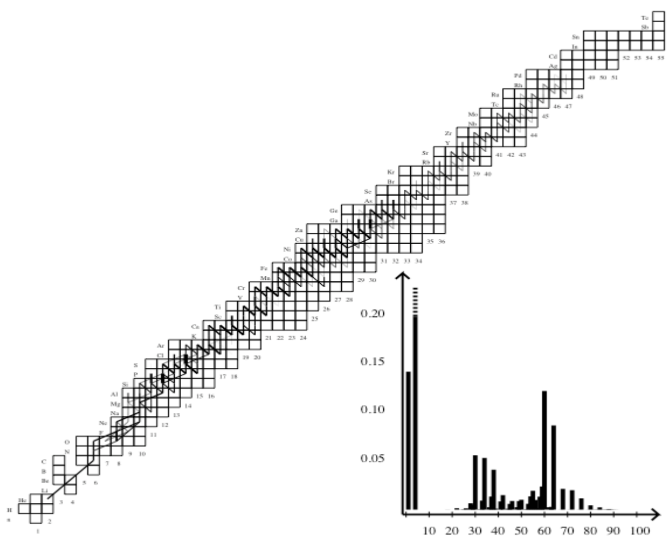

Fig. 18.— Above ignition: $T = 9.93 \cdot 10^8$K, $\rho = 2.43 \cdot 10^5$g/cm^3, $X = 0.143$, $Y = 0.234$, $t = -3.013$s. (see end of §4 for an explanation of the diagram).

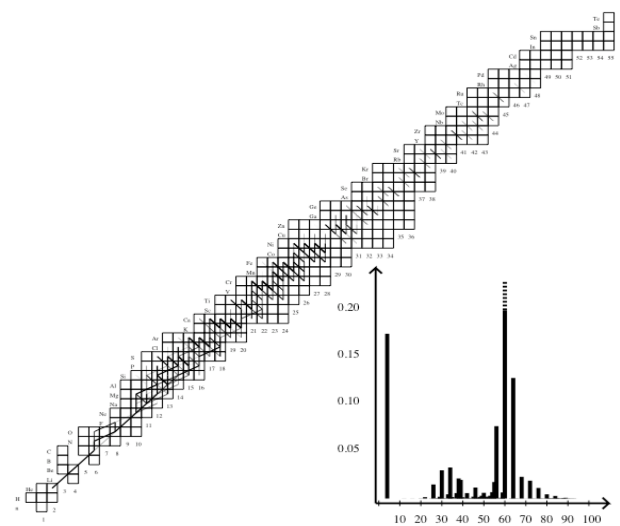

Fig. 19.— Above ignition: $T = 9.62 \cdot 10^8$K, $\rho = 3.54 \cdot 10^5$g/cm^3, $X = 2.5 \times 10^{-5}$, $Y = 0.175$, $X_{60} = 0.346$, $t = 1.476$s. (see end of §4 for an explanation of the diagram).

Evolutionary snapshots of accreted parcel of matter from Fisker et.al. astro-ph/070331 with t=0 at peak surface luminosity.

3D hydrodynamical models of the XRB:Crust Composition Dependencies

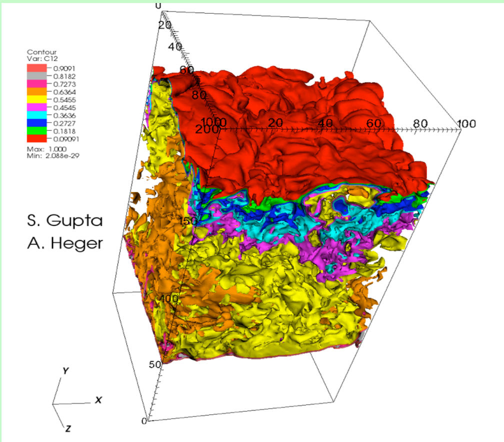

From 1-D multi-zone models of XRB evolution we take compositional and thermodynamic profiles to study the interaction of the H and He convective layers.

The timescale for mixing and burning of H determines how close to the surface the convection penetrates. This affects the rise time of the light curve.

The tail of the light curve depends on how the ^{12}C from the helium layer interacts with the Hydrogen layer - if only a little mixes then the slower rp-process which stalls at the proton drip-line dominates - and upto A=100 elements are produced. This will correspond to an observational signature of slow rise and decay of the lightcurve.

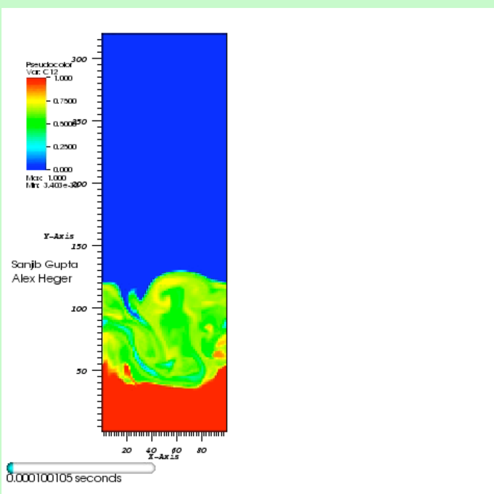

However if most of the ^{12}C mixes then the faster αp-process (also results in a steeper/faster rise to peak luminosity) bypasses the β-decay Waiting Points resulting in pre-Fe-group light elements with short lifetimes that show up as a steep drop-off in the lightcurve when radioactive species are exhausted.

Separation of CNO isotopes from H- Diffusion in MCP

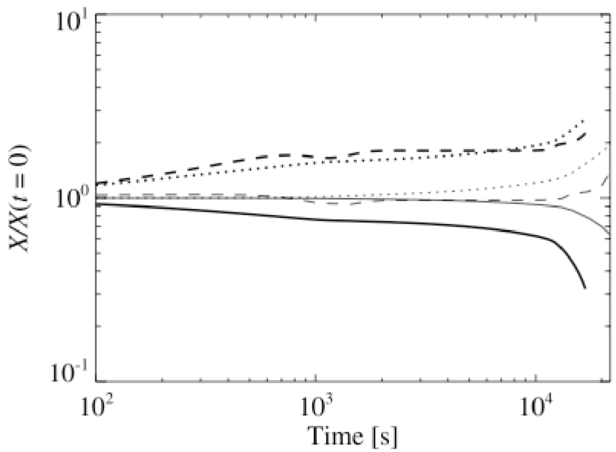

FIG. 2.—Evolution of mass fractions of H (*solid lines*), He (*dotted lines*), and CNO elements (*dashed lines*), normalized to their initial values as a function of Lagrangian time $t = y/\dot{m}$ for $\dot{m} = 0.11\dot{m}_{\rm Edd}$. We show cases when diffusion is (*thick lines*) and is not (*thin lines*) included. The curves terminate when He ignites unstably.

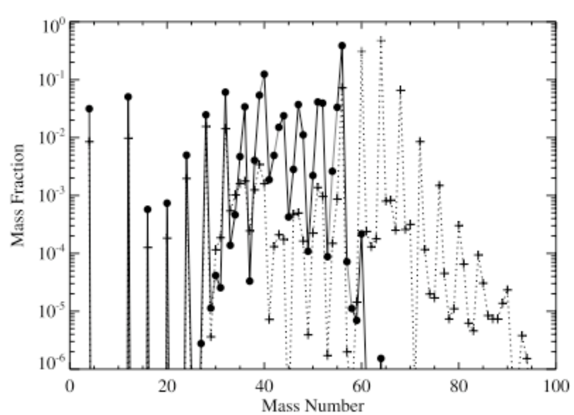

FIG. 13.—Ashes produced by the one-zone burst calculation following unstable He ignition for $\dot{m} = 0.11\dot{m}_{\rm Edd}$. The initial composition is taken from the bottom of the fuel layer at the point at which ^{4}He ignites, for the calculation with (*circles and solid lines*) and without (*plus signs and dotted lines*) sedimentation and diffusion.

A major complication in calculating timescales of nuclear burning is that an ionized stellar plasma in a gravitational field does not move as a composite XRB “ash” parcel : lighter ions float upwards through the ashes and an electric field is generated by the composition gradients that are established (after self-consistently solving for charge neutrality and Hydrostatic Equilibrium).

There is a very large range of plasma conditions under which we need to model this non-equilibrium plasma (inter-) diffusive process: from $\Gamma<1$ ranging to beyond 173, which would correspond to crystallization in the OCP.

Peng et.al. 2007 (ApJ 654:1022-1035, from which figures on left are shown) showed that even for high accretion rates ~$0.1m_{edd}$ the H abundance at the base of the accreted layer is significantly reduced, due to the diffusive separation. Since the timescale for the plasma diffusive separation is of the order of the accretion timescale (time to replenish the accreted column to where is becomes thermally unstable to nuclear reactions), we are missing a crucial piece of the puzzle of H/He/CNO burnings ! The accretion rate at which mixed H/He ignition occurs changes by a factor of 2 simply by coupling the diffusive separation to the nuclear burning evolution.

Finally, a crucial missing ingredient in Superburst ignition is getting enough ^{12}C to survive at 10^9 g cm^{-3} : Sedimentation can substantially change the destruction of ^{12}C by hydrogen burning since it lowers the proton-to-capture-seed ratio in the rp-process and decreases the mean mass of the end composition.

This underscores why we are so interested in sedimentation - the separative process changes **the concentration of nuclear reactants at a depth**, and changes the nuclear burning profile ! Thus the observed energetics could change completely depending on the transport coefficients in our model !

Further, Electron Captures in the Crust make matter increasingly neutron-rich, increasing their susceptibility to gravitational settling vs. the electric field acting on them. The effects will be much stronger than on ^{22}Ne - thus crust nucleosynthesis as we know it could be very different, and further impact the energetics of the crust.

The pure one component plasma (OCP) phase diagram is well known. The liquid solidifies when the ratio of a typical Coulomb energy to the thermal energy kT is $\Gamma \approx 175$ [11]. The parameter Γ is defined,

$$\Gamma = \frac{Z^2 e^2}{aT}, \quad (1)$$

where the ion charge is Ze, the temperature is T, and the ion sphere radius a describes a typical distance between ions, $a = (3/4\pi n)^{1/3}$. Here n is the ion (number) density.

Plasma conditions over the atmosphere and crust of NS range from $\Gamma << 1$ to beyond $\Gamma \sim 200$. However, the current astrophysical models assume $\Gamma << 1$ and describe diffusion as independent binary collisions between Debye-screened particles . This will break down over the range of Γ we are interested in and miss effects such as rapid oscillations in a transient cage formed by nearest neighbors - liquidlike behavior for $\Gamma \sim 10$ (Donko et.al. Phys.Plasmas 10, 1563 (2003)).

The only other approximations in use are classical OCP self-diffusion coefficients for a single representative species (Bildsten and Hall, ApJ 549:L219 which uses the fit of Hansen et.al. Phys.Rev.A 11, 1025(1975)) . This simple power-law fit is extensively discussed in Daligault and Murillo Phys.Rev.E 71, 036408 (2005) and shown to be accurate to only 20% or so to actual MD simulations

$$D = \omega_p a^2 \frac{2.95}{\Gamma^{1.34}},$$

where $\omega_p = \sqrt{4\pi (Ze)^2 n / M}$ is the ion plasma frequency

as crystallization approaches, collective effects play an increasingly important role and diffusion is dominated by many body physics ! We must cover the entire regime of temperature and density conditions that comprise the Neutron Star interior to understand the timescales of non-equilibrium processes.

Coupled Mechanical, Thermal and Nuclear Evolutionary models of the Crust - setting the thermal profile !

* Hydrostatic Equilibrium under GR conditions - Tolman-Oppenheimer-Volkoff equation gives condition for pressure balancing the gravitational force

$$\frac{\partial r}{\partial a} = (4\pi r^2 n)^{-1}\left(1 - \frac{2Gm}{rc^2}\right)$$

$$\frac{\partial m}{\partial a} = \frac{\rho}{n}\left(1 - \frac{2Gm}{rc^2}\right)^{1/2}$$

$$\frac{\partial \Phi}{\partial a} = \frac{Gm}{4\pi r^4 n}\left(1 + \frac{4\pi r^3 P}{mc^2}\right)\left(1 - \frac{2Gm}{rc^2}\right)^{-1/2}$$

$$\frac{\partial P}{\partial a} = -\frac{Gm\rho}{4\pi r^4 n}\left(1 + \frac{P}{\rho c^2}\right)\left(1 + \frac{4\pi r^3 P}{mc^2}\right)\left(1 - \frac{2Gm}{rc^2}\right)^{-1/2}$$

where a = the total number of baryons inside sphere of radius "r" and

- ρ = Mass Density, the potential Φ appears in time-time component of the Schwarzschild metric as e^{Φ/c^2} and governs the redshift of photons and neutrinos. At the stellar surface

$$e^{2\Phi/c^2}\big|_{r=R} = 1 - \frac{2GM}{Rc^2}$$

- Where M=total gravitational mass and $4\pi R^2$ = surface area of the neutron star. Here n = baryon density and m=mass within radius =r
- P(n) is obtained from the EOS by summing the electron, ion and neutron energy density contributions in the outer crust by following the BPS method – electrons are a highly degenerate relativistic Fermi gas,

- Crust EOS is determined pre-ND ($< 4 \cdot 10^{11}$ g/cc) using BPS prescription : sum electron (get pressure from Helmholtz Free Energy Tabulation-partial derivatives) + ionic + lattice (fits) + free neutrons. Compressible liquid-drop model allows for an external neutron gas.
- Free neutrons are present for $n > 3.6 \cdot 10^{-4}\, fm^{-3}$ and dominate the pressure when $n > 0.04\, fm^{-3}$ in which regime the P(n) fit of Negele and Vautherin is used. (Negele & Vautherin, 1973, Nucl.Phys.A,207,298)
- At $n > 0.1\, fm^{-3}$ nuclei dissolve into uniform nuclear matter and we use Akmal et.al. 1998 AV18+dv+UIX results using the Argonne V18 potential with relativistic boost corrections and the TNI =UIX. Neutrons, protons, electrons and where Electron Fermi Energy > rest mass of muon = 105.66 MeV, muons contribute. (Akmal et.al. 1998, Phys. Rev. C vol.58 #3)
- Hyperons/quark matter are not contributors to our EOS.
- For each baryon density we obtain the proton fraction and electron fraction from beta-equilibrium and charge neutrality

$$Y_p = n_p / n$$
$$Y_e = n_e / n$$
$$\mu_n - \mu_p = \mu_e = \mu_\mu$$
$$n_p = n_e + n_\mu$$
$$\rho = nH(n, Y_p, Y_e, Y_\mu) / c^2 = \varepsilon / c^2$$
$$P = n^2 \frac{\partial H}{\partial n} = c^2 \left(-\rho + n \frac{\partial \rho}{\partial n} \right)$$

- P(rho) of AV18+dv+UIX matches Negele and Vautherin at $n = 0.078\, fm^{-3}; P = 0.039\, MeV fm^{-3}$ thus facilitating a smooth transition from crust to core without density discontinuity.
- With P(n) specified integrate structure equations out from fixed central pressure to atmospheric density – compute gravitational mass, adjust central pressure to fit target mass, iterate.

- Steady – State Thermal profile is calculated from solving the entropy and flux equations (L=luminosity, T=proper temperature)

$$e^{-2\Phi/c^2}\frac{\partial}{\partial r}\left(Le^{2\Phi/c^2}\right)-4\pi r^2 n\left(\varepsilon_N-\varepsilon_\upsilon\right)\left(1-\frac{2Gm}{rc^2}\right)^{-1/2}=0$$

$$e^{-\Phi/c^2}K\frac{\partial}{\partial r}\left(Te^{\Phi/c^2}\right)+\frac{L}{4\pi r^2}\left(1-\frac{2Gm}{rc^2}\right)^{-1/2}=0$$

- Where ε_N =nuclear heating from EC and neutron reactions and ε_υ =

crust/core neutrino processes. K=conductivity calculated from composition.

Boundary Conditions on Luminosity are set by flux at r = R (obtained from photospheric calculation, temperature at base of H/He burning shell sets the flux as function of accretion rate) and zero flux at r = 0. Additionally the Luminosity at the crust/core interface must match the core neutrino emissivity.

Electron Transport In Dense Coulomb Plasmas - composition-dependent Conductivities under electron-ion scattering

$$\Gamma(\mathbf{p} \to \mathbf{p}') = \frac{2\pi N}{\hbar^2} \frac{1}{2} \sum_{\sigma\sigma'} |U_{\mathbf{q},\sigma'\sigma}|^2 \, \mathcal{S}(\mathbf{q},\omega), \qquad (1)$$

$$\begin{aligned} \mathcal{S}(\mathbf{q},\omega) &= \frac{1}{2\pi} \int_{-\infty}^{+\infty} \mathrm{d}t \, e^{-i\omega t} S(\mathbf{q},t) \\ &= \frac{1}{2\pi N} \int_{-\infty}^{+\infty} \mathrm{d}t \int \mathrm{d}\mathbf{x} \, \mathrm{d}\mathbf{x}' \, e^{i\mathbf{q}\cdot(\mathbf{x}-\mathbf{x}') - i\omega t} \\ &\quad \times \langle \hat{\rho}^\dagger(\mathbf{x},t) \, \hat{\rho}(\mathbf{x}',0) \rangle_T, \qquad (2) \end{aligned}$$

where N is the total number of ions, $\mathbf{p}$ and $\mathbf{p}'$ are the electron momenta before and after scattering, respectively, $\hbar\mathbf{q} = \mathbf{p}' - \mathbf{p}$, $\hbar\omega = \epsilon' - \epsilon$ is the difference between final and initial electron energies, and $U_{\mathbf{q},\sigma'\sigma}$ is the matrix element of the operator of elementary ei interaction. $\mathcal{S}(\mathbf{q},\omega)$ is the dynamical structure factor of the plasma, the most important quantity of the theory. In the liquid regime, $\hat{\rho}(\mathbf{x},t)$ is the operator of the charge density in units of $Z|e|$: $\hat{\rho}(\mathbf{x},t) = \hat{n}_{\mathrm{I}}(\mathbf{x},t) - n_i$, where $\hat{n}_{\mathrm{I}}(\mathbf{x},t)$ is the ion density operator and $n_i = n_e/Z$ takes account of the compensating electron background with the electron density n_e. In the solid regime, $\hat{\rho}(\mathbf{x},t) = \hat{n}_{\mathrm{I}}(\mathbf{x},t) - \sum_i \delta(\mathbf{x} - \mathbf{R}_i)$ (where $\mathbf{R}_i$ is a lattice vector), i.e. the operator of fluctuations of the charge density.

SCCP of ions in a uniform electron gas (charge compensating) - disordered or in a crystal lattice.

Differential scattering electron-ion rate averaged over initial and summed over final electron spin states on left (from Baiko et.al. 1998)

$$\sigma = \frac{n_e e^2}{m_e^* \nu_\sigma}, \qquad \kappa = \frac{\pi^2 T n_e}{3 m_e^* \nu_\kappa},$$

where $m_e^* = \epsilon_F / c^2$, and

Effective collision frequency $\nu_{\sigma,\kappa} \sim m_e^* Z^2 e^4 L n_i /(k_F^3)$ which sums the differential scattering weighted by statistical phase-space factors over the electron wavevector range to the Fermi Surface

Primary scattering process is electron-impurity (***but need composition dependence***!) not e-p or e-e: so Itoh and Kohyama (ApJ 404, 268) fits are used to compositionally weight the scattering from single-component scattering….assumes there are no clustering/separation effects!

$$\begin{aligned} \langle S \rangle = &\int_0^1 d\left(\frac{k}{2k_F}\right)\left(\frac{k}{2k_F}\right)^3 \frac{S(k/2k_F)}{[(k/2k_F)^2 \epsilon(k/2k_F,0)]^2} - \frac{1.018(Z/A)^{2/3}\rho_6^{2/3}}{1+1.018(Z/A)^{2/3}\rho_6^{2/3}} \\ &\times \int_0^1 d\left(\frac{k}{2k_F}\right)\left(\frac{k}{2k_F}\right)^5 \frac{S(k/2k_F)}{[(k/2k_F)^2 \epsilon(k/2k_F,0)]^2} \end{aligned}$$

where $\hbar k$ is the momentum transferred from the ionic system to an electron, $S(k/2k_F)$ the ionic liquid structure factor, and $\epsilon(k/2k_F, 0)$ the static dielectric screening function due to degenerate electrons. The first term in equation (6) corresponds to the ordinary Coulomb logarithmic term, and the second term is a relativistic correction term.

$$\begin{aligned} \sigma = 8.693 \times 10^{21} \rho_6 \left(\sum_i \frac{X_i}{A_i}\right) &\times \frac{1}{\{1 + 1.018[\sum_i (Z_i/A_i)X_i]^{2/3}\rho_6^{2/3}\}\langle S \rangle} \\ &\times \frac{\langle Z \rangle^2}{\langle (\Delta Z)^2 \rangle} \mathrm{s}^{-1}, \qquad (21) \end{aligned}$$

$$\begin{aligned} \kappa = 2.363 \times 10^{17} T_8 \rho_6 \left(\sum_i \frac{X_i}{A_i}\right) &\times \frac{1}{\{1 + 1.018[\sum_i (Z_i/A_i)X_i]^{2/3}\rho_6^{2/3}\}\langle S \rangle} \\ &\times \frac{\langle Z \rangle^2}{\langle (\Delta Z)^2 \rangle} \mathrm{ergs\ cm^{-1}\ s^{-1}\ K^{-1}}, \qquad (22) \end{aligned}$$

$$\langle Z \rangle \equiv \sum_i x_i Z_i,$$

$$\langle (\Delta Z)^2 \rangle \equiv \sum_i x_i (Z_i - \langle Z \rangle)^2$$

$$x_i \equiv \frac{n_i}{\sum_j n_j}.$$

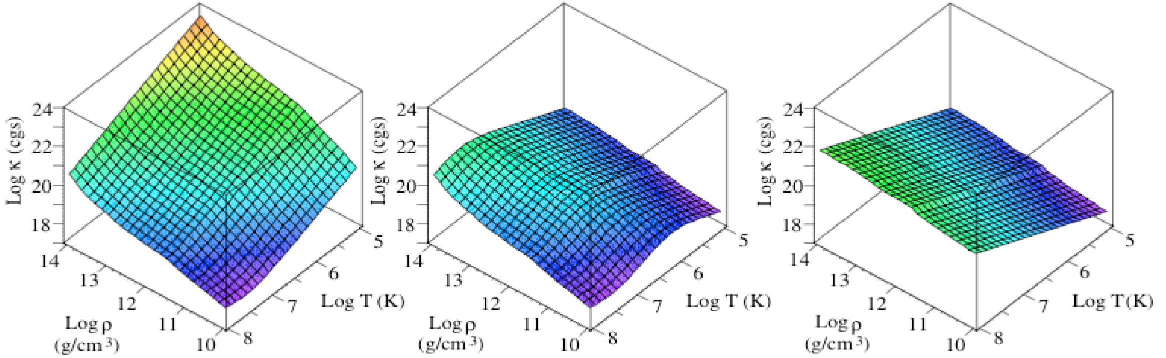

Fig. 1. Thermal conductivity κ_0, in cgs units, versus density ρ and temperature T. The left panel shows the phonon-only contribution $\kappa_{0\,\mathrm{ph}}$, the right one the impurity-only contribution $\kappa_{0\,\mathrm{imp}}$, and the central panel the complete κ_0 (with an impurity concentration $Q_{\mathrm{imp}} = 0.1$).

Deep Crustal Heating Mechanisms and the importance of accurate Nuclear Physics input

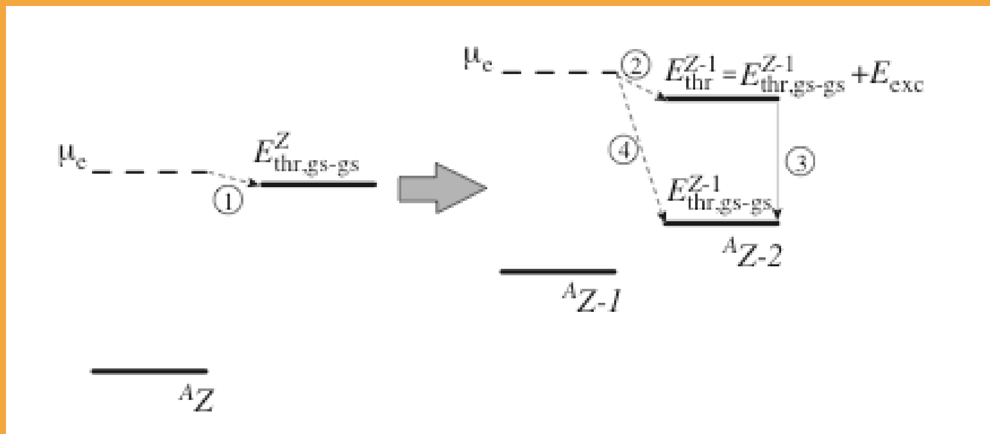

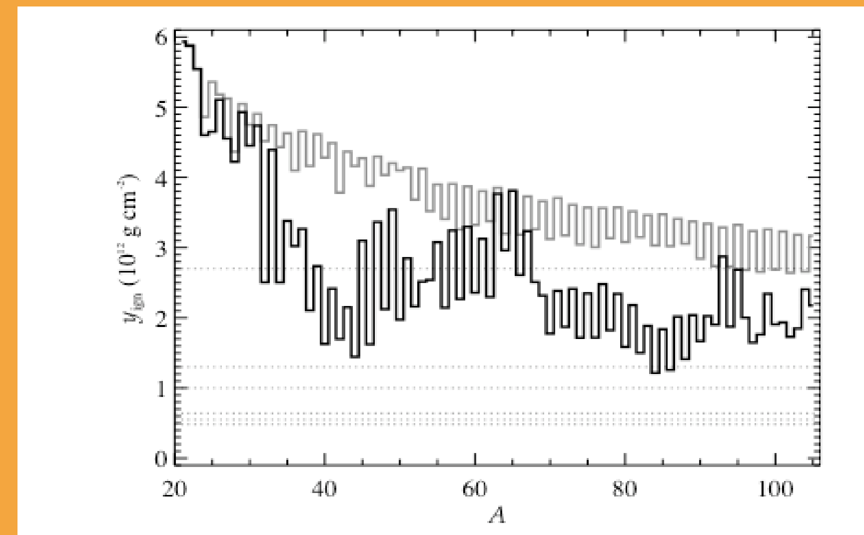

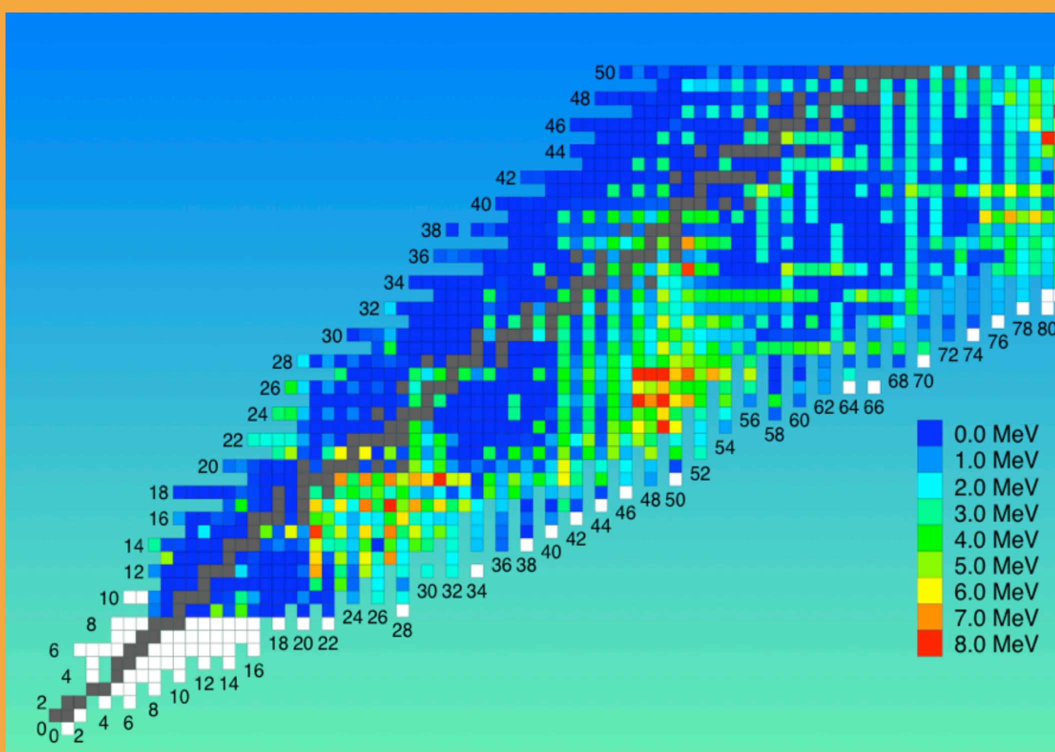

Gupta et.al. 2006 (ApJ 662:1188-1197 co-authors E.F. Brown, H.Schatz, P.Moller and K.-L. Kratz) showed the importance of weak interactions on XRB ash composition for XRSB ignition (nuclear structure effects in reduction in ignition column shown above).

Primary crustal heating process is 2-stage EC on even-even endpoints of XRB At high electron chemical potential (upper left figure) .We incorporate the capture into excited states with accurate B(GT+) calculations from QRPA model (Moller and Randrup, Nuc. Phys. A 514:1-48 (1990)). Parent g.s. only here because of low temp $T_9 < 0.7$,*but* will require parent excited states for WPs (Waiting Points) of XRB.

Plot on left shows color coded excited state energy into which EC predominantly occur: shown are the capture parents-note shell structure effects, odd-even effects, regions where deformations will play an important role.

Importance of B(GT+) shown - now need to incorporate effects from (n,γ) and (EC,*xn*) to determine true heating profile.

CRUST EVOLUTIONMOVIE THEATRE……………………

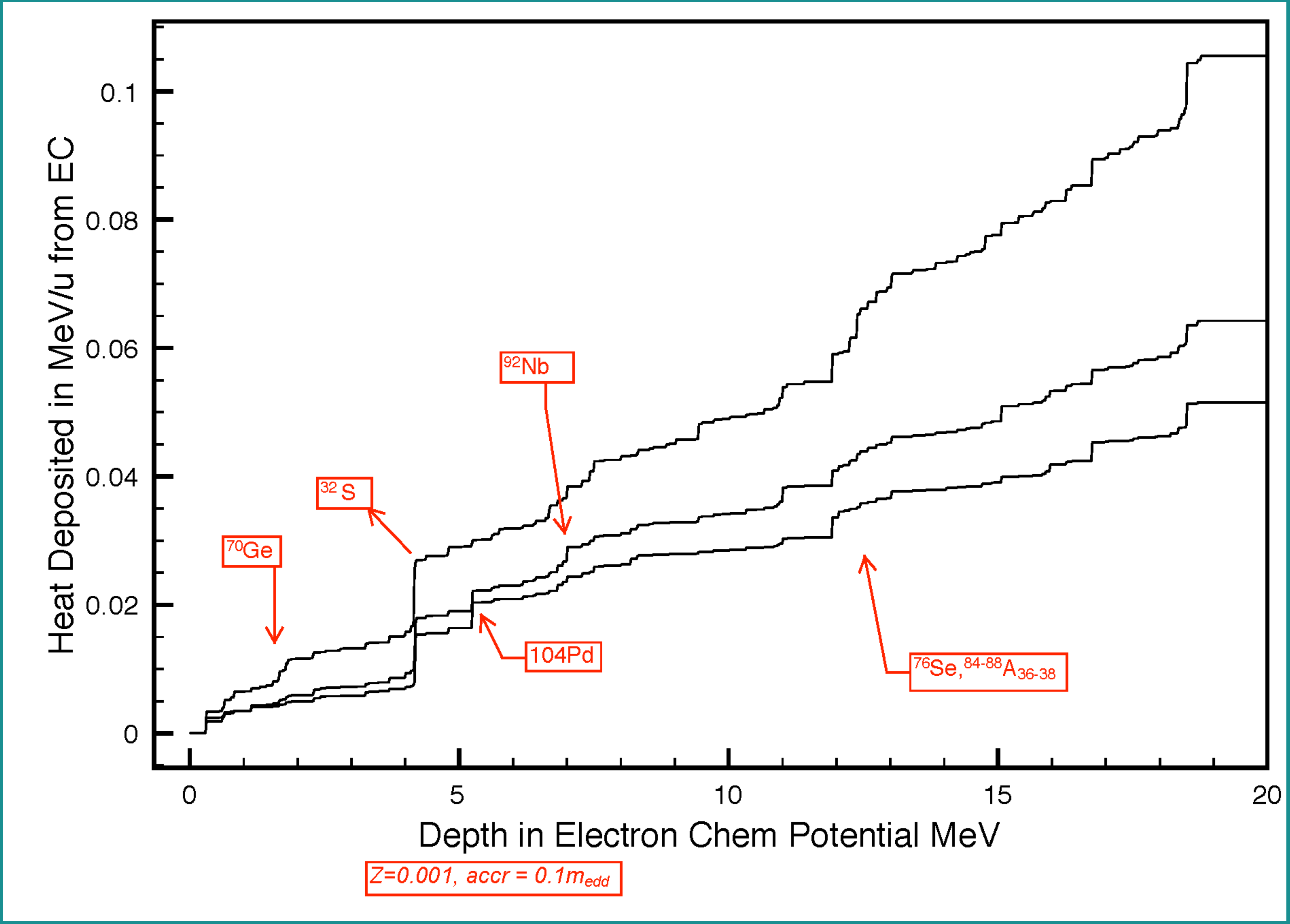

0.1
0.08
0.06
0.04
0.02
0
Heat Deposited in MeV/u from EC
0
5
10
15
20
Depth in Electron Chem Potential MeV
^{70}Ge
^{32}S
^{92}Nb
104Pd
^{76}Se,$^{84\text{-}88}$A$_{36\text{-}38}$
Z=0.001, accr = 0.1m_{edd}

Importance of B(GT+) to XRB *luminosity evolution (lightcurves) + endpoint comp.*

Weak Interaction rates (Positron emission+EC) considerably affect the shapes of the resulting light curves. We also intend to study the role that nuclear isomers play with regards to the rp -process. Though isomers have typically been overlooked in previous studies, their long lifetimes can significantly alter the $T_{1/2}$ of key proton-rich nuclei.

Figures showing changes in lightcurve responses (integrated/bolometric luminosity resulting from nuclear reactions) when key WP nuclei "chokepoints" are given β^+ acceleration/retardation effects from B(GT+) response to ambient temperature/electron chemical potential (electron density).

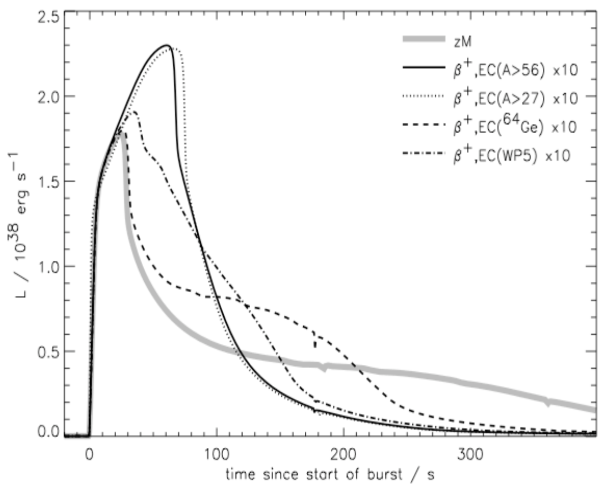

Figure 1: Light curves (bolometric luminosity as function of time) of model X-ray burst. The *thick gray curve* indicates the result for our current "best" data set, the *black lines* show the results if the weak β^+ decay and electron capture (EC) rates were 10× faster, for nuclear mass numbers bigger than $A = 56$ (*solid line*), for masses bigger than $A = 27$ (*dotted*), for the "waiting point" (WP) nucleus ^{64}Ge (*dashed*), and for the five most important waiting points, (^{60}Zn, ^{64}Ge, ^{68}Se, ^{72}Kr, ^{76}Sr; *dash-dotted line*). This increase of the electro-weak reaction rates rates could be due to decay from excited or isomeric nuclear states that are not accounted for in our current rate data set.

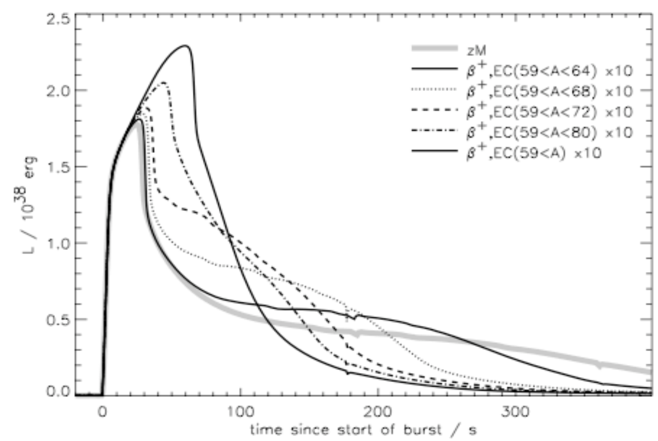

FIG. 19.—Sensitivity of the light curve of the first pulse in model zM to variations along the waiting points in the vicinity of $A = 60$, 64, and 68. The nominal light curve is shown along with the result when all weak rates above $A = 59$ are multiplied by 10 (see Fig. 18; changing $A_{\min}$ from 57 to 59 has no effect). Also shown are the results of progressively adding in accelerations to flows in the mass ranges $A = 60$–63, 64–67, 68–71, and 72–79. Details of the flows for these mass ranges are given in the text. A separate calculation, not shown, in which only the decay rate of ^{64}Ge was accelerated by 10 is virtually indistinguishable from the curve e^+, EC$(59 < A < 68) \times 10$. Factors affecting leakage out of this single nucleus thus dominate the flow from the iron group to ^{68}Se. The "blip" at 180 s is the addition of a new surface zone by accretion.

B(GT+) and the WP of the XRB - Part II

Another very important effect is the effect of β^+ rates in determining the endpoint composition of the rp-process when very proton-rich nuclei are reached and (γ,p) impedes further proton capture in H-burning (connected) cycles. The “ashes” of the rp-process are very important for determining Deep Crustal Heating and therefore the XRSB ignition conditions.

Model zM refers to a specific stellar model in Woosley et.al. 2004 (ApJ 151:75-102) from which these figures are taken. Also refer to Pruet and Fuller 2003 (ApJ Sup.Ser.149:189-203) to see A>65 nuclei treatment with IPM/spherical/logft systematics vs. the QRPA treatment of B(GT+) in Moller and Randrup 1990 which has no model space limitations and naturally incorporates configuration mixing and deformation effects. A<66 rates for Woosley et.al.2004 is from the Shell Model.

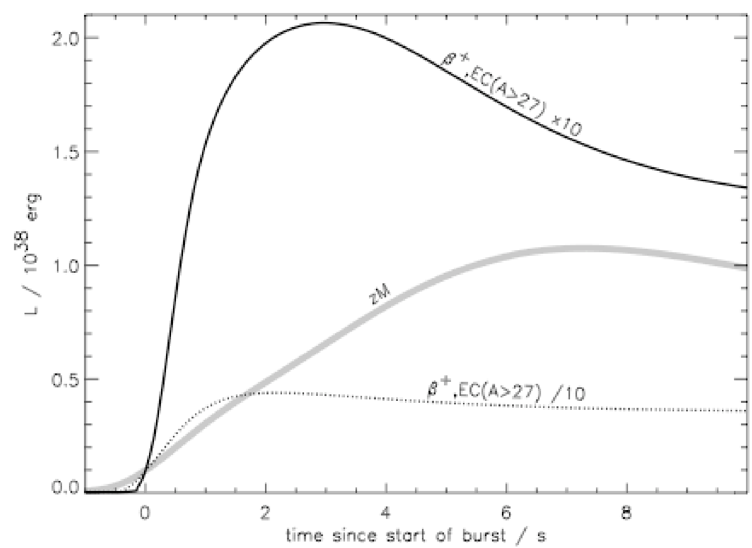

FIG. 20.—Sensitivity of the rise of the light curve of the third pulse in model zM for three choices of weak rates—standard, standard times 10 above $A = 27$, and standard divided by 10 above $A = 28$. Flows affecting the rise time are discussed in the text. Time zero is defined as when each burst reaches 10^{37} ergs s^{-1}. Because this is the third burst, there have been cumulative effects from the altered rates; the critical masses of the burning layers, for example, are not the same (Tables 3–5), nor are the total burst energies.

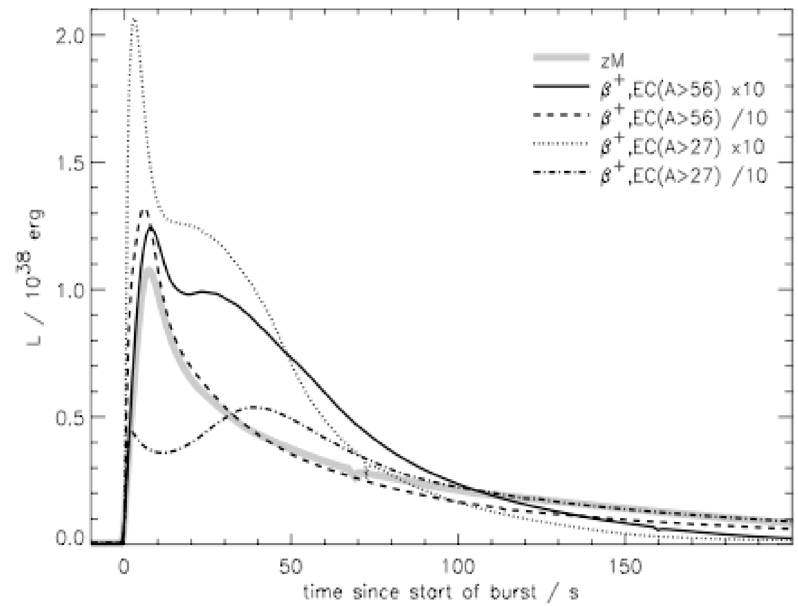

FIG. 21.—Sensitivity of the light curve of the third pulse in model zM to variation in the nuclear physics employed (see Fig. 18). This third burst may be more representative than the first one.